RSC Advances

ROYAL SOCIETY OF CHEMISTRY

www.rsc.org/advances

ZnO/ITO core/shell nanostructure electrodes for future prototype solar cell devices

Mudusu Devika,[1,2] Nandanapalli Koteeswara Reddy,[1,3,#,*] and Charles W. Tu[1,4,*]

[1]Department of Nanobio Materials and Electronics, Gwangju Institute of Science and Technology, Gwangju 500712, Republic of Korea

[2]Department of Aerospace Engineering, Indian Institute of Science, Bangalore 560012, India

[3]Center for Nanoscience and Engineering, Indian Institute of Science, Bangalore560012, India

[4]Department of Electrical and Computer Engineering, University of California, San Diego, La Jolla, CA 92093-0407, USA

[*]Corr. authors: E-mail: dr_nkreddy@rediffmail.com (NKR) and ctu@soe.ucsd.edu (CWT)

[#]Present address: Institute of Chemistry, Humboldt University, Brook-Taylor-Str. 2, 12489 Berlin, Germany.

Abstract: Impact of indium tin oxide (ITO) layer over vertically aligned zinc oxide nanorods (ZnO NRs) has been investigated to consider ITO nanolayer as a transparent conducting oxide electrode (TCOE) for hierarchical heteronanostructure solar cell devices that are having ZnO nanostructures as branches. ZnO/ITO core/shell nanostructures were prepared in two-steps using vapor-liquid-solid and evaporation processes, and further the structures were annealed at various temperatures. Transmission electron microscopic studies show that the as-grown ZnO/ITO

structures consist of amorphous ITO shell on single crystalline ZnO cores, whereas the structures annealed above 300 ^{o}C consist of single crystalline ITO shell. ITO layers deposited ZnO NRs exhibit a small red-shift in ZnO near-band-edge emission as well as optical band gap. The electrical measurements carried out on single ZnO/ITO core/shell NR under dark and UV light showed excellent thermionic transport properties. From these investigations it is emphasized that ITO nanolayers could be used as TCO electrode for prototype ZnO based hierarchical solar cell devices.

Keywords: Type-II core/shell nanostructures; Wide band gap materials; ZnO/ITO interface properties; Optical properties.

1. Introduction

Semiconductor heteronanostructures (HNSs) have recently received great attention due to their unique properties, and thereby multifunctional applications.[1, 2] In principle, HNSs are three types: Type-I (straddling gap), Type-II (staggered gap), and Type-III (broken gap) structures, and have their own advantages in different fields.[3] Significantly, Type-I structures have more advantages in the development of high-yield light emission devices, whereas Type-II structures have key applications in the field of photovoltaics (PV). For example, Sungjee Kim et al. have synthesized both Type-I as well as Type-II quantum dot (QD) structures and observed good

quantum yield enhancement in Type-I structures (20%), and shrinkage in Type-II structures (4%).[4] In this direction, a variety of heteronanostructures including InAs/InP,[5] InAs/CdSe,[6] CdSe/CdS,[7, 8] CdSe/CdS/$Zn_{0.5}Cd_{0.5}S$/ ZnS,[9] Si/ZnO,[10-12] Si/SiGe,[13, 14] GaAs/GaP,[15, 16] TiO_2/SnO_2,[17, 18] ZnO/Ge,[19-21] and CdSe/Si[22] structures have been synthesized by using multidisciplinary methods, and explored interesting physical and chemical properties. On the other hand, a few groups have also fabricated PV devices using various heteronanostructures and noticed considerable light conversion efficiency.[23-26]

In general zinc oxide (ZnO) exhibits wurtzite crystal structure and wide band gap of ~3.37 eV. High exciton binding energy (60 meV) makes this material as a good candidate for the development of room temperature ultra-violet (UV) lasers.[27] Recently, one dimensional (1D) ZnO nanostructures play a vital-role in the development of advanced and multifunctional devices due to their large surface-to-volume ratio, tunable electrical and optical properties, and the photon confinement effect.[28-32] On the other hand, as compared to simple nanostructures, ZnO heteronanostructures are received particular interest due to their huge surface area and typical optical properties.[33-37] For example, composite ZnO nanostructures with different polymers or metal nanoparticles exhibit a significant enhancement in their electrical and optoelectrical performances.[38-45] A few groups have synthesized Type-II heterostructures using p-type silicon (Si) nanowires as cores and n-type ZnO nanorods as branches (i.e., Si/ZnO hetero-hierarchical

nanostructures), and proposed as appropriate candidates for the development of prototype PV devices.[12, 46, 47] In order to realize such a novel hetero-hierarchical nanostructures based PV devices (see supporting information (SI)-1) it is most important to identify an appropriate transparent conducting electrode layer for the effective collection of photogenerated carriers at active cores of the device.

Indium tin oxide (ITO) is one of the most widely used transparent conducting oxide (TCO) materials for the development of efficient PV devices because of its high electrical conductivity and optical transparency along with excellent moisture resistance.[48] As compared to ZnO, it exhibits low electrical resistivity, high visible transmittance, and relatively high work function.[49] Based on the energy band diagram of ZnO/ITO (see SI-1 Fig. 1b) it can be underlined that ITO can be a good Ohmic and TCO contact for ZnO material. In this view, there have been a large number of reports on ZnO based devices using ITO as TCO. However, it is difficult to understand the interfacing properties of ZnO/ITO structures by using microscale data. Thus, it is important to understand the interfacing between ITO and ZnO nanostructures and also the impact on the physical properties of ZnO NRs. In this direction, we carried out a systematic investigation to study the impact of ITO nanolayer growth over ZnO NRs, and annealing on the physical properties of ZnO NRs and reported here.

2. Experimental procedure

Synthesis: ZnO/ITO NR structures have been realized in two-steps. Initially, ZnO NRs were synthesized by chemical vapor deposition (CVD) technique using vapor-liquid-solid (VLS) method on Au coated c-plane Al_2O_3 substrates (one set of samples has been prepared on transparent both sides polished sapphire substrates). Here, the Au film with a thickness of ~3 nm was deposited by e-beam evaporation system. The growth of ZnO NRs was carried out at a temperature and pressure of 950 ^oC and 20 Torr under Ar and O_2 flow with a rate of 100 and 2 sccm, respectively, in the duration of 5 minutes.[45] Further, ITO layer with a thickness of 50 nm was deposited at room temperature (RT) by e-beam evaporation at the vacuum pressure of 10^{-6} Torr by maintain continuous rotation. After this, the as-grown ZnO/ITO NR structures were annealed on digital hotplate at three typical temperatures of 100, 300, and 500 ^oC in air ambient for 10 minutes.

Characterization: Structural properties and phase purity of the as-grown and heat treated nanostructures were studied by powder X-ray diffraction (XRD) using Cu $K\alpha_1$ radiation in the diffraction range of 10-70°. Field emission scanning electron microscopy (FESEM) and energy dispersive analysis of X-rays (EDAX) techniques were used to examine the surface morphology and chemical composition of the structures, respectively. Advanced techniques such as transmission electron microscopy (TEM), high-resolution TEM (HRTEM), scanning-TEM

(STEM), selected area electron diffraction (SAED), energy dispersive spectroscopy (EDS) were used for further confirmation of crystallographic and chemical composition properties. Here, in order to partially remove the ITO layer, ZnO/ITO heterostructures were subjected to a vigorous sonication for better ZnO/ITO interface analysis. The quality of ZnO/ITO structures was also studied using UV-Micro Raman spectrometry in the frequency range from 70 to 1500 cm^{-1}. The optical behavior of nanostructures was estimated using photoluminescence (PL) spectroscopy and UV-Vis-NIR spectrophotometer. PL measurements were carried out in the wavelength range 350-650 nm using a He-Cd laser with an excitation wavelength of 325 nm, and the absorbance studies were measured in the wavelength range of 300-2500 nm with the incident light parallel to the growth direction of ZnO NRs. Finally, M1/ZnO/ITO/M2 devices (M1=Ni/Au and M2=Au) were fabricated using photolithography and I-V characteristics were studied at RT (SI-2).

3. Results and discussion

The as-grown and 100 ^{o}C annealed ZnO/ITO structures appear brownish in color and also opaque, whereas the structures annealed above this temperature appear as same as bare ZnO NRs, i.e. white in color. These changes in appearance of ZnO/ITO nanostructures mainly attributed to the variation of oxygen content in ITO layer since it has been deposited at RT.

Morphology and crystal structure of ZnO NRs: Surface morphology studies, Fig. (1a and 1b),

show that ZnO NRs on sapphire substrates are dense and vertically aligned with uniform surface morphology. These ZnO NRs have an average length of 5 μm and their diameter varied between 50 and 100 nm. EDAX analysis, Fig. 1c, reveals that ZnO NRs probably consist of stoichiometric chemical composition since the Zn and O atomic% ratio of NRs is found to be ~1. The XRD studies, Fig. 1d, revealed that most of the ZnO NRs are preferentially oriented along the (002) planes since the calculated interplanar spacing (d-spacing) value of the dominant peak diffracted at $2\theta = 34.4^{o}$ (d = 0.261 nm) exactly matched with the hexagonal ZnO (JCPDS Card No: 36-1451). The full width at half maximum (FWHM) value of the preferential peak is found to be ~0.25^{o}. This considerably low value emphasize the crystalline quality of CVD grown ZnO NRs.[50] Further, a minor peak diffracted at 16.84^{o} (d = 0.523 nm) belongs to ZnO (001) plane; whereas the other minor peaks diffracted at 30.9, 38.02, 42.08, and 64.7^{o} belong to Au catalyst and sapphire substrate, respectively.

Morphology and crystal structure of ZnO/ITO core/shell structures: FESEM analyses of ITO deposited ZnO NRs show that ITO layer on ZnO NRs consists of uniformly embedded nanoparticles like morphology and it appears rough in nature. The diameter of these core/shell NRs varied between 150 and 200 nm. Upon annealing ZnO/ITO core/shell NRs, the morphology of ITO shell on ZnO NR cores is unchanged and however, its surface roughness gradually decreased (see the insets of Fig. 2). The XRD spectra of as-grown and 100 ^{o}C annealed ZnO/ITO

core/shell structures consist of similar structural characteristics as bare ZnO NRs. The structures annealed above 100 ^{o}C showed two new weak diffraction peaks at 30.4 and 50.9^{o}, which can be clearly noticed from the elaborated XRD spectra (20-30^{o}) of untreated and treated ZnO/ITO structures shown in Fig. 3 and SI-3. These newly evolved diffraction peaks can be assigned to $(12\bar{1})$ and $(12\bar{4})$ planes of rhombohedral ITO since the calculated d-spacing values of these peaks (0.293 and 0.179 nm) match with the JCPDS data of ITO (Card No: 89-459). On the other hand, after the deposition of ITO layer, the FWHM value of ZnO NRs drastically increased and it further increased when ZnO/ITO structures annealed at 100 ^{o}C. Interestingly, above this annealing temperature, the FWHM value slightly decreased (see SI-4). The changes in the crystalline properties of ITO shell deposited on ZnO cores with annealing temperature are clearly observed in TEM studies, which are discussed below.

TEM analysis of ZnO NRs and ZnO/ITO core/shell NRs: HRTEM studies on as-grown ZnO NRs, Fig. 4a, show that the surface of as-grown ZnO NRs is slightly rough in nature, whereas their lattice fringes are clear and distinguishable. The d-spacing values, calculated from the fast Fourier transformation (FFT) analysis of Fig. 4a, is found to be 0.259 and 0.162 nm, which belong to (002) and (110) planes of the hexagonal ZnO. It indicates that CVD grown ZnO NRs on sapphire substrates are clear single crystalline in nature and are preferentially grown along the <001> direction. The SAED analysis also confirms the same, Fig. 4b. The EDS studies performed on a

single ZnO NR show that the as-grown ZnO NRs solely consist of Zn and O elements in the atomic ratio of 1:1. It indicates that the single crystalline ZnO NRs grown by CVD method have excellent chemical stoichiometry between the constituent elements.

HRTEM and FFT analyses of as-grown ZnO/ITO core/shell structure, left inset of Fig. 4c, reveal that vertically aligned ZnO NR cores have uniformly covered ITO shell, and the interface between core and shell is nearly smooth and abrupt. The average thickness of ITO shell on ZnO NR is found to be 45 nm. The d-spacing value between adjacent lattice planes is about 0.524 nm, which corresponds to (001) planes of hexagonal ZnO. The FFT analysis of ZnO/ITO interface, right inset of Fig. 4c, demonstrates that the as-deposited ITO shell on ZnO NRs consists of amorphous nature (see SI-5). Further, the SAED pattern of as-grown ZnO/ITO core/shell NR, Fig. 4d, clearly emphasized that a thin amorphous ITO shell is well grown on single crystalline ZnO cores. The measured radius of this amorphous ring is found to be 0.292 nm and thus, it probably belongs to $(12\bar{1})$ orientation of rhombohedral ITO.

A detailed composition analysis was carried out on a single ZnO/ITO core-shell NR by elemental mapping with STEM-EDS. Fig. 4e shows a STEM image of as-grown ZnO/ITO heterostructure, and the recorded mapping images of Zn (pink), O (green), In (indigo), and Sn (blue) are shown in Fig. 4(f-i), respectively. This clearly reveals that ITO layer on ZnO NR cores

is uniform and well distributed. On the other hand, the spatial distribution of elemental contents across the ZnO/ITO heterostructure (see inset of Fig. 5), obtained by a line-scanning elemental mapping of Zn, O, In, and Sn, are shown in Fig. 5. It clearly demonstrates that ZnO/ITO nanostructures have well-defined compositional profile. Further, the profile of Zn shows comparatively sharp peak at the center, whereas the profiles of O, In, and Sn show broad peaks spread over the whole spectrum. As expected, the oxygen content in the ZnO/ITO NRs is evenly distributed throughout the diameter of heterostructure since it both the structures contain oxygen. The thickness of ITO shell and the diameter of ZnO NR have been measured from Fig. 5 and are found to be ~40 and ~75 nm, respectively, which are comparable with FESEM and HRTEM data.

HRTEM and SAED images along with their corresponding FFT images of annealed ZnO/ITO core/shell NRs at 100, 300, and 500 ^{o}C are shown in Fig. 6(a-f). Theses analyses show that the ZnO/ITO structures annealed at 100 ^{o}C still contain amorphous ITO shell over single crystalline ZnO cores. However, the SAED image of 100 ^{o}C annealed ZnO/ITO structures exhibited an additional diffraction ring, which belongs to $(12\bar{4})$ orientation of rhombohedral ITO since the radius of the ring is found to be ~0.179 nm. For further increase of annealing temperature, the amorphous ITO shell over ZnO core gradually converted into single crystalline structure. This can be clearly noticed from Fig. 6(c-f). Finally, the ZnO/ITO structures annealed at 500 ^{o}C consist of purely single crystalline rhombohedral ITO shell that was grown along the

$< 12\bar{1} >$ direction on the hexagonal facets of ZnO NRs. These results are consistent with the data observed in XRD studies and imply that the as-deposited ITO layer on ZnO NRs is amorphous, and upon annealing it becomes crystalline. Most of the ITO crystallites on ZnO NRs formed at higher annealing temperatures are preferentially oriented along the $< 12\bar{1} >$ direction.

Micro-Raman studies: The Raman spectra of as-grown ZnO NRs, Fig. 7a, exhibited two distinguishable peaks at 100±1 and 438±2 cm^{-1}, which are commonly observed peaks in the wurtzite structured ZnO.[51-53] These peaks belong to nonpolar optical phonon modes and can be identified as low- and high- frequency branches of E_2 mode (i.e. E_2-low and E_2-high modes), which are consistent with the earlier data on ZnO nanostructures.[54-56] Usually, the E_2-low and -high modes associated with the vibration of heavy zinc sublattice and oxygen atoms, respectively.[57, 58] Here, the ratio between E_2-low and -high modes of bare ZnO NRs is found to be ~0.61, which indicates that the as-grown ZnO NRs have excellent crystalline quality.[59] On the other hand, a few additional second-order peaks noticed at 540±1 (E_2-high+E_2-low), 811±1 (E_1-transverse optical+E_2-high), 1154±1, and 1324±1 cm^{-1} are attributed to overtones or combination of first-order modes.[60-62]

After the deposition of ITO layer, the overall intensity of the whole spectrum drastically decreased (Fig. 7b), whereas the E_2-low/E_2-high peaks ratio increased. Upon annealing the

ZnO/ITO structures, this trend is continued and the structures annealed at 100 ^{o}C exhibited a maximum E_2-low/E_2-high ratio of 1.95 (Fig. 7c). A further increase in annealing temperature, the E_2-low/E_2-high ratio gradually decreased (Fig. 7f), whereas the background of the Raman spectrum increased (Fig. 8d-e). These results indicate that as compared to bare ZnO NRs, the crystalline quality of as-grown as well as heat treated ZnO/ITO core/shell NRs slightly poor, probably attributed to the presence of amorphous ITO layer. However, the crystalline quality of the structures treated at higher temperatures (> 100 ^{o}C) slightly improved and obtained better quality at the annealing temperature of 500 ^{o}C.[59] This trend is similar to the results observed in XRD as well as TEM analyses. On the other hand, ZnO/ITO structures annealed at ≥100 ^{o}C exhibited a new peak at 336±2 cm^{-1}. This peak is attributed to (E_2-high) - (E_2-low) multiphonon mode, which is probably originated from the surface states of ZnO/ITO structures.[63, 64]

Photoluminescence studies: PL spectra of all the structures exhibited a strong emission peak in ultra-violet (UV) region along with a few defect-related sharp emission doublet peaks on a broad visible band, as shown in Fig. 8(a-e). The spectrum of as-grown ZnO NRs consist of a sharp UV peak located at around 380.9 nm (~3.26 eV) and minor doublet peaks at (486, 490), (541, 546), (576, 579), 587, 611, and 631 nm. Here, the background under broad band peak is high, and the energy gap between the each doublet emission peak is about 20 meV. Compared to the PL spectrum of bare ZnO NRs, the intensity of as-grown and 100 ^{o}C annealed ZnO/ITO structures is

low, and however, the peaks in the visible region emerged as clearer and sharper. Above this annealing temperature, the background under the visible band again increased. The UV peak usually arises from the electron-hole recombination between the conduction band (CB) and valence band (VB), i.e., near-band-edge (NBE) emission.[65, 66] The peaks observed at various wavelengths in the visible region, according to the hypotheses proposed to understand the origin of defect-related emission mechanism,[38, 67, 68] probably generated from radiative recombination of photo-generated carriers at various ionized charge states including oxygen interstitials (O_i), zinc interstitials (Zn_i), zinc vacancies (V_{Zn}), and oxygen vacancies (V_o) that exist between VB and CB (see SI-6). Besides this, a minor peak from as-grown and annealed ZnO/ITO structures observed at a wavelength of ~593 nm (~2.09 eV). Noticeably, above 100 ^oC its intensity also increased with increase of annealing temperature (see SI-7). The presence of this peak is probably attributed to ITO nanoparticles since the In-doped SnO_2 nanowires exhibit similar luminescence peak between 1.9 and 2.0 eV.[69]

The emission quality of structures has been estimated by calculating the intensity ratio between the UV and 541 nm visible peaks (I_{UV}/I_{541}), and the variation of I_{UV}/I_{541} ratio with annealing temperature is shown in Fig. 8f. Upon the deposition of ITO layer, the emission quality of as-grown ZnO NRs degraded, and it decreased further when the structures were annealed at 100 ^oC. However, the structures annealed above 100 ^oC showed slight improvement in their emission

quality. After the deposition of ITO layer, UV peak position of ZnO NRs shifted towards lower energies by 5 meV and this shift continued with annealing of ZnO/ITO structures upto 100 ^{o}C. This gradual red-shift in UV peak position with annealing temperature (upto 100 ^{o}C) is mainly attributed to the presence of tensile-strain in ZnO lattice due to ITO layer as shell.[13, 15, 16, 70-76] In the case of as-grown ZnO/ITO NRs, the presence of amorphous ITO layer on ZnO cores strongly imposes high anisotropic strain, that probably cause for a red-shift in UV peak position of ZnO NRs. Upon annealing the ZnO/ITO structures upto 100 ^{o}C, the formation of uniform and well-sealed amorphous ITO layer on ZnO cores probably increases the shell-induced-strain and causes for further red-shift in UV peak position. However, at higher annealing temperatures, the formation of highly-crystalline ITO structures probably enforces a low strain on ZnO NRs and as a result, gradual blue-shift in the position of UV peak. The same trend is observed in optical absorbance studies of ZnO/ITO core/shell nanostructures, as shown in Fig. 9.

Optical properties: ZnO and all ZnO/ITO NRs consist of similar optical behavior at lower (<400 nm) as well as at higher wavelengths (>1500 nm) (Fig. 9a). Around the visible wavelengths, ITO coated ZnO NRs exhibited slightly higher absorbance than the as-grown ZnO NRs, and further the same tread continued with the increase of annealing temperature upto 100 ^{o}C. Above this annealing temperature, the absorbance of the structures gradually decreased, i.e. ZnO/ITO structures annealed at 500 ^{o}C are more transparent to visible light. These changes in absorbance

properties of ZnO/ITO NRs mainly attributed to the nature of ITO layer, as observed in TEM studies. On the other hand, the enlarged absorbance versus wavelength spectra at around 385 nm (Fig. 9b) show that all the ZnO/ITO core/shell structures consist of different optical absorption edges than the as-grown ZnO NRs. The optical band gap (E_g) of all the structures was determined using the standard thin films procedure and E_g has been determined by extrapolating the linear portion of the $(\alpha h\nu)^2$ versus $h\nu$ plot (Fig. 9c) to $(\alpha h\nu)^2=0$. Thus, the as-grown ZnO NRs showed a direct optical band gap of 3.26 eV, which is comparable with the NBE emission peak of ZnO NRs. After the deposition of ITO shell, as noticed in PL studies, the E_g value deceased, and it further decreased with increase of annealing temperature upto 100 ^oC (Fig. 9d). Above this temperature, the E_g value slightly increased.

A gradual decrease in emission intensity as well as transmittance of ZnO NRs with the deposition of ITO layer strongly attributed to the presence of oxygen deficient amorphous ITO layer. The as-grown ITO layer on ZnO NRs is partially opaque and as a result, it prevents the light penetration as well as emission. On the other hand, the presence of native defect states in ITO layer as well as at ZnO/ITO interface also reduces the overall intensity of PL emission and light transmission since these defect states act as non-radiative recombination centers and hinder (or absorbs) the light from ZnO cores.[77] However, the gradual formation of single crystalline ITO

layer on ZnO cores at higher annealing temperatures transmit as well as emit the light since recrystallized ITO layer is transparent.

Fabrication and characterization of ZnO/ITO NR device: ZnO/ITO NRs annealed at 500 ^{o}C were adopted for the fabrication of diodes using two different Ohmic contacts with help of photolithographic bilayer mask (SI-2). The device performance was estimated under dark and light (4 W 350 nm UV light). The schematic diagram and FESEM image of n-N junction (n-ZnO/N-ITO) diode are shown in Fig. 10 (a and b). Typical current versus voltage (I-V) characteristics of the as-grown device under dark and illumination are shown in Fig. 10c. Under both the conditions, the device exhibited nearly linear I-V characteristics. It indicates that the junction formed between ZnO and ITO structures is Ohmic and maximum current flow through the single NR device is in the order of μA. However, the current flow through the device under light is 11 time higher than the dark, which is attributed to the excitation of carriers in ZnO NRs. The series resistance between two electrodes under dark and light are found to be 8.3 and 6.5 MΩ, respectively. These electrical characteristics reveal that the as-grown device consists of thermionic carrier transport mechanism and shows that ITO can act as very good TCOE layer for ZnO nanostructures.

4. Conclusions

In view of future prototype solar cell devices using ZnO nanostructures as branches and ITO nanolayer as TCOE, the impact of ITO nanolayer over ZnO NRs and annealing of ZnO/ITO structures on the physical properties of ZnO NRs was investigated. The growth of ITO nanolayer on vertically aligned ZnO NRs is uniform and has slightly rough surface. Upon annealing, the roughness of ITO layer is decreased and formed smooth core/shell structures. Structural analyses reveal that the ZnO/ITO core/shell structures annealed at 500 ^{o}C consist of single crystalline crystallites, whereas the as-grown and annealed ZnO/ITO structures at lower temperatures consist of amorphous ITO layer over highly crystalline ZnO NRs. From the composition analysis it is noticed that all the core/shell nanostructures, except 500 ^{o}C annealed ones, consist of oxygen deficient ITO shell on ZnO cores. As compared to other structures, highly crystalline ZnO/ITO core/shell structures exhibited good light emission and transmission properties. Further, the devices fabricated with annealed ZnO/ITO NRs at 500 ^{o}C exhibited excellent thermionic electrical transport properties under dark as well as light environments. It indicates that the formation of ITO nanolayers over ZnO NRs (or even branches) can act as excellent TCOE since the junction formed between ZnO and ITO is non-rectifying junction. From these results, therefore, it is concluded that the impact of crystalline ITO layer over ZnO NRs is marginal and the electrical transportation in ZnO/ITO core/shell structures is thermionic. Thus, ZnO/ITO core/shell configuration can be adopted as an electrode with appropriate p-type material for transmission of light and collection of charge carriers.

Acknowledgment: This research was supported by the WCU (World Class University) program through the National Research Foundation of Korea funded by the Ministry of Education, Science and Technology (R31-10026). The authors are highly thankful to Mr. Jun, SEM operator, GIST, and Dr. Moon, TEM operator, KBSI, Gwangju for their consistent help in our samples analysis. Reddy and Devika are thankful to J. -W. Kang and for their timely support while executing this work.

Figure captions:

Fig. 1: (a) and (b) Low and high magnification FESEM images, (c) EDAX profile, and (d) XRD spectrum of ZnO NRs on c-plane sapphire substrate.

Fig. 2: FESEM images of (a) ITO deposited ZnO NRs (left inset represents a single as-grown ZnO/ITO NR and right inset shows the top-surface view of ZnO/ITO NRs) and (b) annealed ZnO/ITO structures at 500 ^{o}C (inset shows a single annealed ZnO/ITO NR), respectively.

Fig. 3: Elaborated XRD spectra of (a) as-grown, (b) 100, (c) 300, and (d) 500 ^{o}C annealed ZnO/ITO core/shell nanostructures (inset of (a) shows the elaborated XRD spectrum of bare ZnO NRs).

Fig. 4: (a) HRTEM and (b) SAED images of as-grown ZnO NR. (c) HRTEM and (d) SAED images of as-grown core/shell nanostructure. The corresponding left insets show the bright field TEM image of NRs and right insets show FFT image taken from HRTEM image. And (e) STEM image, EDS maps of (f) Zn, (g) O, (h) In, and (i) Sn signals, respectively recorded from the as-grown core/shell structures.

Fig. 5: EDS line scanned profiles of Zn, O, In, and Sn elements recorded on as-grown ZnO/ITO NRs (inset shows the STEM images of core/shell NRs).

Fig. 6: HRTEM and SAED images of annealed ZnO/ITO structures at (a) and (b) 100 (insets show from left to right: the FFT images taken from HRTEM image on ITO, interface between ZnO/ITO, and ZnO NR), (c) and (d) 300 (insets show the FFT image taken from the whole HRTEM image-top and bright field TEM image of ZnO/ITO NR-bottom), and (e) and (f) 500 ^{o}C (insets show bright filed TEM image of ZnO/ITO NRs-left and FFT images taken from ZnO NR and from their interface- right top and bottom, respectively).

Fig. 7: Raman spectrum of (a) as-grown ZnO NRs, (b) as-grown and annealed ZnO/ITO NRs at (c) 100, (d) 300, (e) 500 ^{o}C, and (f) variation of E_2-low/E_2-high ratio of ZnO/ITO structures with

annealing temperature.

Fig. 8: Photoluminescence spectra of (a) as-grown ZnO, (b) as-grown and annealed ZnO/ITO NR structures at (c) 100, (d) 300, and (e) 500 ^{o}C and (f) variation of I_{UV}/I_{541} ratio and NBE peak position with structure condition of ZnO/ITO NRs.

Fig. 9: (a, b) Absorption versus wavelength spectra of ZnO and all ZnO/ITO core/shell NRs, (c) $(\alpha h\nu)^2$ versus photon energy plots of all the sample, and (d) variation of optical band gap with structure condition of ZnO/ITO NRs.

Fig. 10: ZnO/ITO core/shell NR based prototype device: (a) Schematic diagram, (b) FESEM image, and (c) current-voltage plot measured under dark and UV light.

References:

1. L. Vayssieres, *Abstr Pap Am Chem S*, 2012, **244**.
2. Y. J. Lin, S. Zhou, R. Liu, G. B. Yuan, S. W. Sheehan and D. W. Wang, *Abstr Pap Am Chem S*, 2011, **242**.
3. J. Tersoff, *Phys Rev B*, 1984, **30**, 4874.

4. S. Kim, B. Fisher, H. J. Eisler and M. Bawendi, *J Am Chem Soc*, 2003, **125**, 11466.
5. Y. Sakuma, M. Ozeki, O. Ueda and T. Ashino, *T Mrs Jap*, 1994, **19**, 157.
6. M. Ben-Lulu, D. Mocatta, M. Bonn, U. Banin and S. Ruhman, *Nano Lett*, 2008, **8**, 1207.
7. M. Dalela, H. Singh, U. Soni and S. Sapra, *2013 International Conference on Advanced Nanomaterials and Emerging Engineering Technologies (Icanmeet)*, 2013, 144.
8. U. Soni, A. Pal, S. Singh, M. Mittal, S. Yadav, R. Elangovan and S. Sapra, *Acs Nano*, 2014, **8**, 113.
9. S. S. Xu, H. B. Shen, C. H. Zhou, H. Yuan, C. S. Liu, H. Z. Wang, L. Ma and L. S. Li, *J Phys Chem C*, 2011, **115**, 20876.
10. S. H. Baek, J. S. Park, Y. I. Jung, I. K. Park and J. H. Kim, *J Nanosci Nanotechno*, 2013, **13**, 6359.
11. S. K. Chong, E. L. Lim, C. C. Yap, W. S. Chiu, C. F. Dee and S. A. Rahman, *Sci Adv Mater*, 2014, **6**, 782.
12. M. Devika, N. K. Reddy, M. Prashantha, K. Ramesh, S. V. Reddy, Y. B. Hahn and K. R. Gunasekhar, *Phys Status Solidi A*, 2010, **207**, 1864.
13. X. Y. Liu, W. L. Liu, X. B. Ma, S. L. Lv, Z. T. Song and C. L. Lin, *Appl Surf Sci*, 2010, **256**, 3499.
14. S. A. Mala, L. Tsybeskov, D. J. Lockwood, X. Wu and J. M. Baribeau, *Appl Phys Lett*, 2013, **103,** 033103.
15. M. Montazeri, M. Fickenscher, L. M. Smith, H. E. Jackson, J. Yarrison-Rice, J. H. Kang, Q. Gao, H. H. Tan, C. Jagadish, Y. N. Guo, J. Zou, M. E. Pistol and C. E. Pryor, *Nano Lett*, 2010, **10**, 880.
16. D. G. Santiago-Perez, C. Trallero-Giner, R. Perez-Alvarez, L. Chico, R. Baquero and G. E. Marques, *J Appl Phys*, 2012, **112,** 084322.
17. P. Chetri, P. Basyach and A. Choudhury, *Chem Phys*, 2014, **434**, 1.
18. A. Y. Pang, X. Sun, H. C. Ruan, Y. F. Li, S. Y. Dai and M. D. Wei, *Nano Energy*, 2014, **5**, 82.
19. C. P. Liu, Y. T. Hung, J. S. Tsai, G. J. Huang and T. R. Jeng, *Jpn J Appl Phys 1*, 2007, **46**, 7365.
20. H. Sadeghi, A. Zolanvar, A. Ranjgar and R. Norouzi, *Plasmonics*, 2014, **9**, 327.
21. X. Huang and J. L. Coffer, *The Journal of Physical Chemistry C*, 2010, **114**, 22019.
22. S. Liu, P. Cheng and H. Wang, *Opt Lett*, 2012, **37**, 1814.
23. R. Bose, G. Manna, S. Jana and N. Pradhan, *Chem Commun*, 2014, **50**, 3074.
24. S. K. Han, M. Gong, H. B. Yao, Z. M. Wang and S. H. Yu, *Angew Chem Int Edit*, 2012, **51**, 6365.
25. J. Xie, X. G. Yang, S. Zhou and D. W. Wang, *Acs Nano*, 2011, **5**, 9225.
26. M. H. Abdullah, L. N. Ismail, M. H. Mamat, M. Z. Musa and M. Rusop, *Microelectron Eng*, 2013, **108**, 138.

27. M. H. Huang, S. Mao, H. Feick, H. Q. Yan, Y. Y. Wu, H. Kind, E. Weber, R. Russo and P. D. Yang, *Science*, 2001, **292**, 1897.
28. T. Voss, G. T. Svacha, E. Mazur, S. Muller, C. Ronning, D. Konjhodzic and F. Marlow, *Nano Lett*, 2007, **7**, 3675-3680.
29. N. K. Reddy, M. Devika and C. W. Tu, *Rsc Adv*, 2014, **4**, 37563.
30. X. Huang, J. L. Coffer, J. A. Paramo and Y. M. Strzhemechny, *Cryst Growth Des*, 2009, **10**, 32.
31. O. Lupan, V. M. Guérin, I. M. Tiginyanu, V. V. Ursaki, L. Chow, H. Heinrich and T. Pauporté, *Journal of Photochemistry and Photobiology A: Chemistry*, 2010, **211**, 65.
32. G. Xiuquan, Q. Yinghuai and Z. Yulong, *Rare Metal Materials and Engineering*, 2014, **43**, 1296.
33. Z. L. Wang, *J Phys-Condens Mat*, 2004, **16**, R829.
34. L. E. Greene, M. Law, B. D. Yuhas and P. D. Yang, *J Phys Chem C*, 2007, **111**, 18451.
35. M. Law, L. E. Greene, J. C. Johnson, R. Saykally and P. D. Yang, *Nat Mater*, 2005, **4**, 455.
36. M. Law, L. E. Greene, A. Radenovic, T. Kuykendall, J. Liphardt and P. D. Yang, *J Phys Chem B*, 2006, **110**, 22652.
37. N. K. Reddy, M. Devika, N. Shpaisman, M. Ben-Ishai and F. Patolsky, *J Mater Chem*, 2011, **21**, 3858.
38. C. S. Lao, P. M. Gao, R. Sen Yang, Y. Zhang, Y. Dai and Z. L. Wang, *Chem Phys Lett*, 2006, **417**, 358.
39. C. S. Lao, M. C. Park, Q. Kuang, Y. L. Deng, A. K. Sood, D. L. Polla and Z. L. Wang, *J Am Chem Soc*, 2007, **129**, 12096.
40. T. W. Chen, Y. H. Zheng, J. M. Lin and G. N. Chen, *J Am Soc Mass Spectr*, 2008, **19**, 997.
41. J. M. Lin, H. Y. Lin, C. L. Cheng and Y. F. Chen, *Nanotechnology*, 2006, **17**, 4391.
42. J. M. Lin, Y. Z. Zhang, Z. Z. Ye, X. Q. Gu, X. H. Pan, Y. F. Yang, J. G. Lu, H. P. He and B. H. Zhao, *Appl Surf Sci*, 2009, **255**, 6460.
43. L. Lin, J. M. Lin, J. H. Wu, S. C. Hao and Z. Lan, *Mater Res Innov*, 2010, **14**, 370.
44. C. S. Wang, H. Y. Lin, J. M. Lin and Y. F. Chen, *Appl Phys Express*, 2012, **5,** 062201.
45. M. Devika, N. K. Reddy, J. W. Kang, S. J. Park and C. W. Tu, *Ecs Solid State Lett*, 2013, **2**, P101.
46. C. W. Cheng, B. Yan, S. M. Wong, X. L. Li, W. W. Zhou, T. Yu, Z. X. Shen, H. Y. Yu and H. J. Fan, *Acs Appl Mater Inter*, 2010, **2**, 1824.
47. K. S. Son, D. H. Lee, J. W. Choung, Y. B. Pyun, W. Il Park, T. Song and U. Paik, *J Mater Res*, 2008, **23**, 3403.
48. M. S. Hwang, B. Y. Jeong, J. Moon, S. K. Chun and J. Kim, *Mater Sci Eng B-Adv*, 2011, **176**, 1128.
49. H. L. Hetnagel, Dawar, A. L., Jain, A. K., Jagadishi, C., *Superconducting Transparent thin Films*, IOP Publishing, Bristol and Philadelphia, 1995.

50. X. Liu, X. H. Wu, H. Cao and R. P. H. Chang, *J Appl Phys*, 2004, **95**, 3141.
51. T. A. Harriman, Z. Bi, Q. X. Jia and D. A. Lucca, *Appl Phys Lett*, 2013, **103,** 121904.
52. I. Lorite, P. Diaz-Carrasco, M. Gabas, J. F. Fernandez and J. L. Costa-Kramer, *Mater Lett*, 2013, **109**, 167.
53. C. C. Wang, C. M. Fu and Y. M. Hu, *Surf Coat Tech*, 2013, **231**, 307.
54. J. H. Yang, M. Gao, L. L. Yang, Y. J. Zhang, J. H. Lang, D. D. Wang, Y. X. Wang, H. L. Liu and H. G. Fan, *Appl Surf Sci*, 2008, **255**, 2646.
55. G. S. Wu, T. Xie, X. Y. Yuan, Y. Li, L. Yang, Y. H. Xiao and L. D. Zhang, *Solid State Commun*, 2005, **134**, 485.
56. R. N. Gayen, A. Rajaram, R. Bhar and A. K. Pal, *Thin Solid Films*, 2010, **518**, 1627.
57. U. Ozgur, Y. I. Alivov, C. Liu, A. Teke, M. A. Reshchikov, S. Dogan, V. Avrutin, S. J. Cho and H. Morkoc, *J Appl Phys*, 2005, **98,** 041301.
58. J. S. Thakur, G. W. Auner, V. M. Naik, C. Sudakar, P. Kharel, G. Lawes, R. Suryanarayanan and R. Naik, *J Appl Phys*, 2007, **102,** 093904.
59. B. Zhou, A. V. Rogachev, Z. B. Liu, D. G. Piliptsou, H. J. Ji and X. H. Jiang, *Appl Surf Sci*, 2012, **258**, 5759.
60. H. K. Yadav, K. Sreenivas, V. Gupta and R. S. Katiyar, *J Raman Spectrosc*, 2009, **40**, 381.
61. K. Samanta, S. Dussan, R. S. Katiyar and P. Bhattacharya, *Appl Phys Lett*, 2007, **90,** 261903.
62. T. C. Damen, S. P. S. Porto and B. Tell, *Phys Rev*, 1966, **142**, 570.
63. T. L. Phan, R. Vincent, D. Cherns, N. X. Nghia and V. V. Ursaki, *Nanotechnology*, 2008, **19,** 475702.
64. B. Q. Wang, X. D. Shan, Q. Fu, J. Iqbal, L. Yan, H. G. Fu and D. P. Yu, *Physica E*, 2009, **41**, 413.
65. E. M. Wong and P. C. Searson, *Appl Phys Lett*, 1999, **74**, 2939.
66. B. D. Yao, Y. F. Chan and N. Wang, *Appl Phys Lett*, 2002, **81**, 757.
67. B. X. Lin, Z. X. Fu and Y. B. Jia, *Appl Phys Lett*, 2001, **79**, 943.
68. Y. Dai, Y. Zhang, Y. Q. Bai and Z. L. Wang, *Chem Phys Lett*, 2003, **375**, 96.
69. X. Y. Xue, Y. J. Chen, Y. G. Liu, S. L. Shi, Y. G. Wang and T. H. Wang, *Appl Phys Lett*, 2006, **88,** 013115.
70. X. B. Chen, Y. B. Lou, A. C. Samia and C. Burda, *Nano Lett*, 2003, **3**, 799.
71. O. Demichel, V. Calvo, P. Noe, B. Salem, P. F. Fazzini, N. Pauc, F. Oehler, P. Gentile and N. Magnea, *Phys Rev B*, 2011, **83,** 245443.
72. I. A. Goldthorpe, A. F. Marshall and P. C. McIntyre, *Nano Lett*, 2009, **9**, 3715.
73. Y. S. Koo, K. M. Song, N. Hur, J. H. Jung, T. H. Jang, H. J. Lee, T. Y. Koo, Y. H. Jeong, J. H. Cho and Y. H. Jo, *Appl Phys Lett*, 2009, **94,** 032903.
74. P. F. Lu, C. Sun, H. W. Cao, H. Ye, X. X. Zhong, Z. Y. Yu, L. H. Han and S. M. Wang, *Solid State Commun*, 2014, **178**, 1.

75. P. Wojnar, M. Zielinski, E. Janik, W. Zaleszczyk, T. Wojciechowski, R. Wojnar, M. Szymura, L. Klopotowski, L. T. Baczewski, A. Pietruchik, M. Wiater, S. Kret, G. Karczewski, T. Wojtowicz and J. Kossut, *Appl Phys Lett*, 2014, **104,** 103113.
76. S. Y. Yang, D. Prendergast and J. B. Neaton, *Nano Lett*, 2010, **10**, 3156.
77. K. Ip, M. E. Overberg, Y. W. Heo, D. P. Norton, S. J. Pearton, S. O. Kucheyev, C. Jagadish, J. S. Williams, R. G. Wilson and J. M. Zavada, *Appl Phys Lett*, 2002, **81**, 3996.

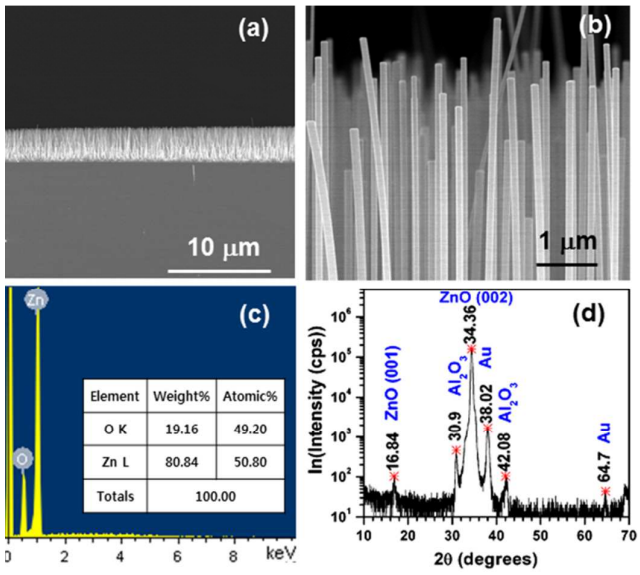

Figure 1/10

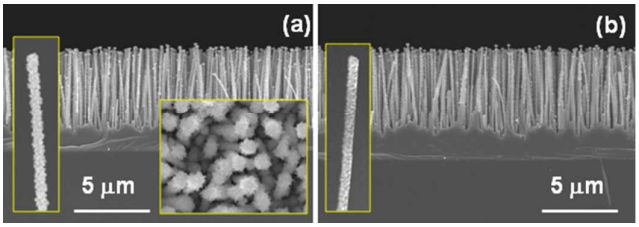

Figure 2/10

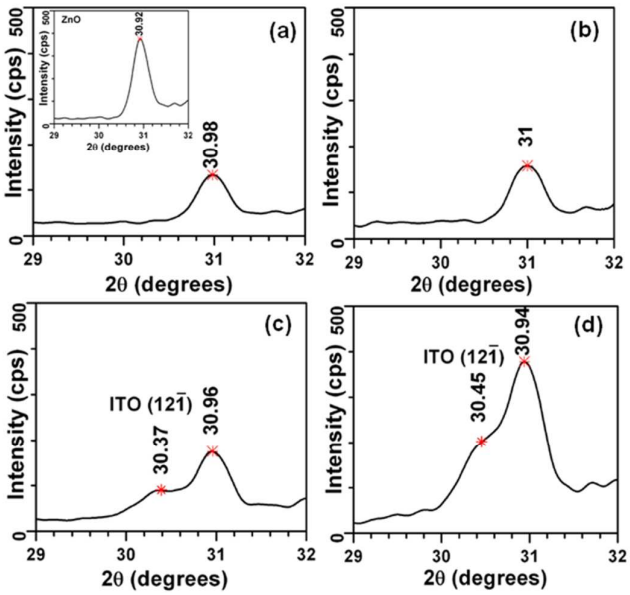

Figure 3/10

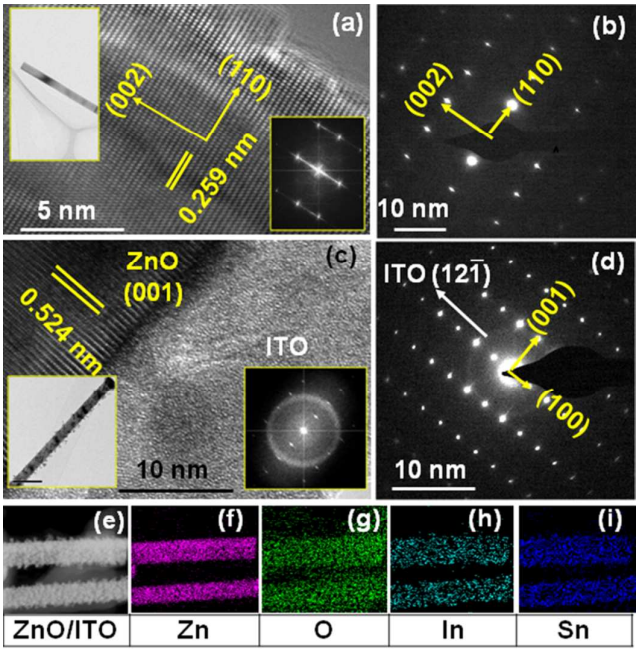

Figure 4/10

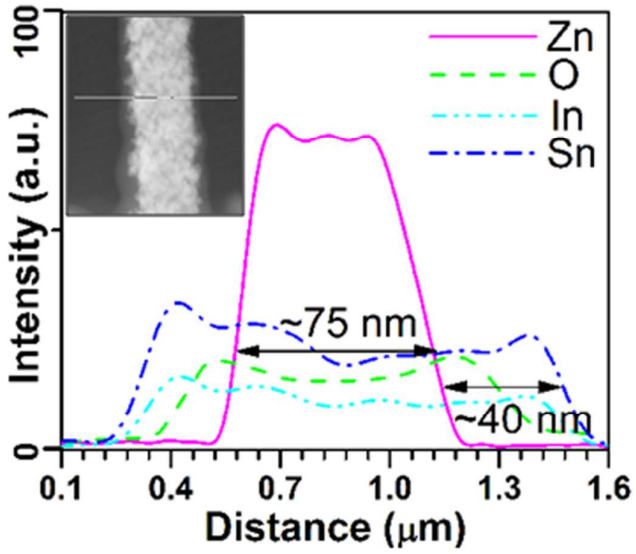

Figure 5/10

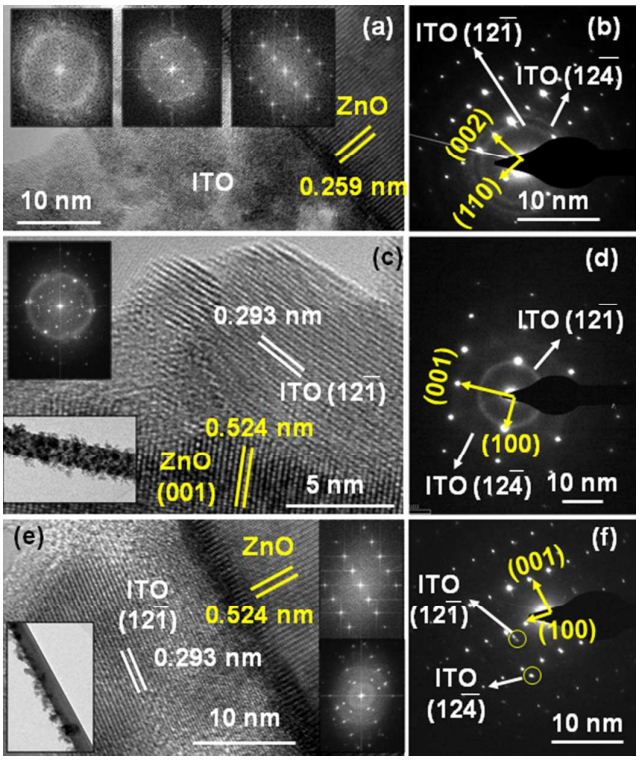

Figure 6/10

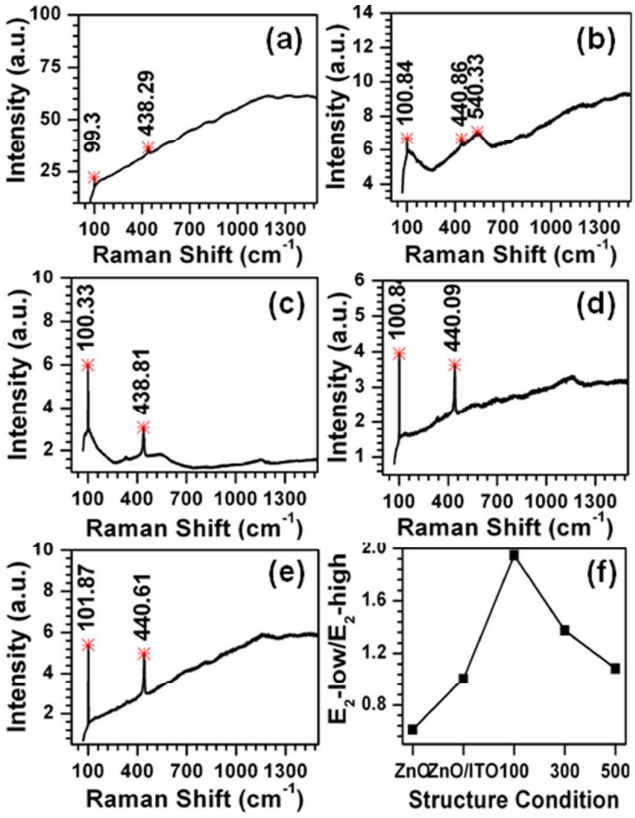

Figure 7/10

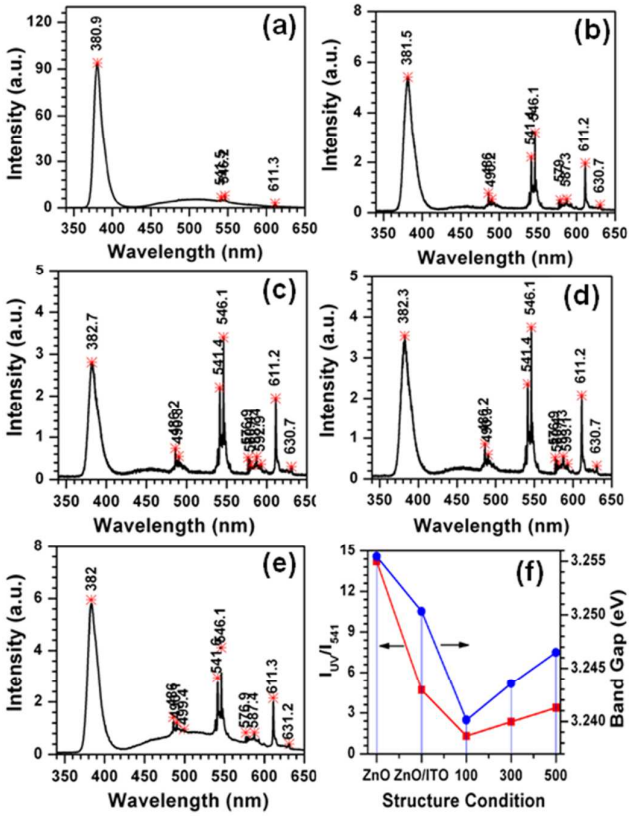

Figure 8/10

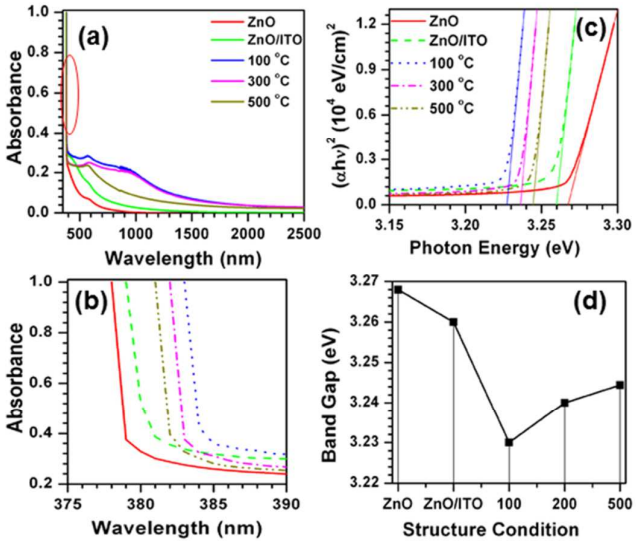

Figure 9/10

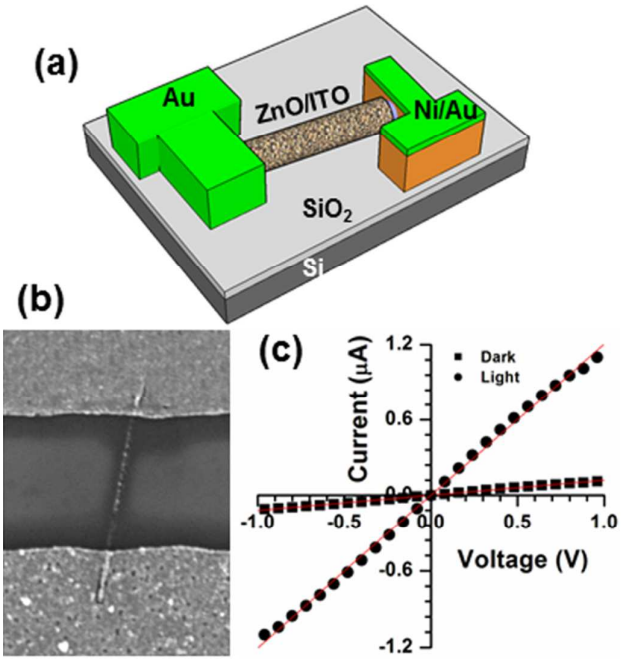

Figure 10/10